NMR Studies of the POU-Specific DNA-Binding Domain of Oct-1: Sequential ^1H and ^{15}N Assignments and Secondary Structure†

Michel Cox,‡ Niek Dekker,‡,§ Rolf Boelens,‡ C. Peter Verrijzer,§ Peter C. van der Vliet,§ and Robert Kaptein*,‡

Bijvoet Center for Biomolecular Research, Utrecht University, Padualaan 8, 3584 CH Utrecht, The Netherlands, and Laboratory for Physiological Chemistry, Utrecht University, Vondellaan 24a, 3521 GG Utrecht, The Netherlands

Received January 5, 1993

ABSTRACT: The ^1H and ^{15}N resonances of the POU-specific DNA-binding domain of transcription factor Oct-1 have been assigned sequentially using two-dimensional homo- and heteronuclear NMR techniques, as well as three-dimensional heteronuclear NMR techniques, including TOCSY, 2D NOE, and NOESY-HMQC experiments. A number of typical short- and medium-range NOE contacts, as well as amide proton exchange data, gave evidence for the presence of four α-helices, in the peptide segments 1–19, 23–34, 40–49, and 54–71, which are connected by short loops of irregular structure. Interestingly, the second helix contains three glycine residues and the fourth helix a proline in the middle of the helix. Although the regular pattern of hydrogen bonds in the fourth helix is interrupted, due to the absence of an amide proton in proline, the helix is remarkably stable. All four helices are amphipathic, which suggests a packing of the apolar sides of the helices in the folded structure of the protein.

The POU domain is a conserved region of about 160 amino acids present in a family of eukaryotic transcription factors, that play regulatory roles in development [reviewed in Ruvkun and Finney (1991), Rosenfeld (1991), and Schöler (1991)]. The ubiquitous transcription factor Oct-1, containing a POU domain, is a 90-kDa nuclear protein that binds to the octamer sequence (Sturm et al., 1988). This DNA sequence is an essential component of promoters and enhancers of several cellular genes like histone H2B, U1 and U2, small nuclear RNAs, and immunoglobulin light and heavy chains. The POU domain has been shown to be involved in DNA binding, whereas regions outside this domain serve transactivating functions. Moreover, Oct-1 and even the separate POU domain stimulate replication of adenovirus DNA (Verrijzer & Van der Vliet, 1993).

The POU domain is a bipartite structure consisting of an N-terminal POU-specific (POU_s)[1] domain of 72 amino acid residues and a C-terminal POU homeodomain (POU_{hd}) of 60 residues connected via a 15–27-residue spacer region (Ingraham et al., 1990; Verrijzer et al., 1990a,b; Kristie & Sharp, 1990; Botfield et al., 1992). Both the POU_s and POU_{hd} are needed for sequence-specific DNA binding with high affinity (Verrijzer et al., 1992). For the isolated POU_{hd}, DNA binding has been demonstrated, albeit with different specificity and with lower affinity than the intact POU domain. For the isolated POU_s subdomain, sequence-specific DNA binding could also be demonstrated, but the affinity toward DNA is very low (Verrijzer et al., 1992).

Until now, no structural analysis has been reported for the POU domain. The amino acid sequence of the POU_{hd} shows sequence homology (25%) with homeobox-related homeodomains. The homeodomains *Antennapedia*, *engrailed* and *Mat*α*2* have been structurally characterized with NMR (Qian et al., 1989) and X-ray crystallography (Kissinger et al., 1990; Wolberger et al., 1991). The homeodomain is a triple-helical structure, in which the third helix is the DNA recognition helix. This helix binds in the major groove of the DNA, making base pair specific interactions. Comparison of the three structures has indicated a high structural similarity among these homeodomains. Since many of the essential amino acids in the fold among the homeodomains and the POU_{hd} are conserved, a similar structure is expected for the POU homeodomain.

Here we report the NMR analysis of the POU-specific domain of Oct-1. This POU_s subdomain shows an even stronger sequence homology with other members of the POU protein family, implying that the 3D structure of POU_s is well conserved. We have assigned the ^1H and ^{15}N resonances in the protein using homonuclear 2D NMR and heteronuclear 3D NMR. On the basis of the sequential and medium-range NOE connectivity patterns, we report the secondary structural elements in the sequence.

MATERIALS AND METHODS

Protein Expression and Purification. The Oct-1 DNA sequence coding for POU_s residues 284–359 (designated residues 1–76 in this paper) was cloned from pBSoct1+ (Sturm et al., 1988) by PCR using Vent-polymerase (Biolabs). The PCR product was cut using the *Nde*I and *Bam*HI restriction enzymes and cloned into the pET 15b-expression vector (Novagen). The sequence was verified by double-stranded DNA sequencing. The protein contained an N-terminal His_6-tag (Janknecht et al., 1991) combined with a thrombin protease cleavage site, which allowed the removal of the histidine fusion part after the purification. The POU_s was expressed in the *Escherichia coli* strain BL21(DE3) using the protocol as

† The investigations were supported by the Netherlands Foundation for Chemical Research (SON) with financial aid from the Netherlands Organization for Scientific Research (NWO).

* Address correspondence to this author.

‡ Bijvoet Center for Biomolecular Research.

§ Laboratory for Physiological Chemistry.

[1] Abbreviations: 1D, one dimensional; COSY, correlated spectroscopy; DQF-COSY, double quantum filtered correlated spectroscopy; DTT, dithiothreitol; EDTA, ethylenediamine tetraacetic acid; HMQC, heteronuclear multiple quantum correlation; HSQC, heteronuclear single quantum correlation; NMR, nuclear magnetic resonance; NOE, nuclear Overhauser enhancement; NOESY, nuclear Overhauser enhancement spectroscopy; PMSF, phenylmethanesulfonyl fluoride; POU_{hd}, POU homeodomain; POU_s, POU-specific domain; ppm, parts per million; RT, room temperature; TOCSY, total correlation spectroscopy; TPPI, time-proportional phase increment.

0006-2960/93/0432-6032$04.00/0

described by Studier et al. (1990). After 4 h of induction, cells from a 3-L culture were harvested by centrifugation (4 krpm, 30 min at 4 °C). The pellet was suspended in 100 mL of lysis buffer containing 50 mM Tris, pH 8.0, 250 mM NaCl, 1 mM DTT, 1 mM EDTA, 1 mM PMSF, and 10 mM metabisulfite. Thirty milligrams of lysozyme was added, and the suspension was stirred for 30 min at 4 °C, followed by a freeze–thaw step. Subsequently, 3 mg of DNase I was added, and the suspension was stirred for 45 min at RT. The solution was centrifuged at 10 krpm for 30 min at RT. The clear supernatant containing the His-tagged POU_s was purified by Ni-NTA affinity chromatography (Qiagen). Lysate corresponding to 1 L of starting culture with around 30 mg of POU_s protein was loaded on a 10-mL column of Ni-NTA, which was preequilibrated with buffer A (10 mM Tris, pH 8.0, 1 mM PMSF, and 1 mM β-mercaptoethanol). The column was washed with 40 mL of buffer A. The His-tagged POU_s protein was eluted by applying a linear gradient of 0–0.5 M imidazole (pH 7) in buffer A. The protein eluted rather broad at 0.1–0.3 M imidazole, and elution was monitored at 280 nm. The fractions of the three affinity chromatography runs containing POU_s were combined and dialyzed overnight against buffer B (30 mM NaOAc, pH 5.0, and 1 mM DTT) to which was added glycerol to a final concentration of 10% (v/v), 1 mM PMSF, and 1 mM metabisulfite in a dialysis bag with a molecular mass cutoff of 2 kDa (Sigma). The dialysate was loaded on a 10-mL fast-flow S-Sepharose column (Pharmacia), preequilibrated with buffer B. The column was developed with a linear NaCl gradient (0–1.5 M) in buffer B, and the His-tagged POU_s eluted at 1.2 M NaCl. At this stage, the protein was free of protease inhibitors, and migrated as one band in Coomassie-stained 15% polyacrylamide gel electrophoresis. The fractions containing protein were pooled and dialyzed overnight against 10 mM Tris, pH 8.0, 1 mM DTT, and 10% glycerol (v/v). The resulting 80-mL protein solution with a concentration range of 1 mg/mL was incubated with 1% thrombin (w/w) (Roche) at RT for 2 h. Thereafter, the solution was acidified to pH 5.0 using 0.1 N HCl, and applied to the 10-mL fast-flow S-Sepharose column, preequilibrated with buffer B. The column was developed with a linear NaCl gradient (0–1.5 M) in buffer B, and POU_s eluted as one single peak at 0.8 M NaCl. The final yield of POU_s was 26 mg/L. Protein purity was checked with polyacrylamide gel electrophoresis. The uniformly ^{15}N-labeled protein was obtained in essentially the same way, from *E. coli* cells grown on a minimal medium, with 0.5 g/L $^{15}NH_4Cl$ as the sole nitrogen source. The overall yield in this case, however, was 22 mg of purified POU_s from a 3-L culture. Protein concentrations were determined by optical density measurement at 280 nm using the calculated value of OD_{280} = 0.67 for a 1 mg/mL POU_s solution.

Sample Preparation. The POU_s was concentrated to 4 mM typically in 0.1 M NaCl/5 mM DTT, using Amicon dialyzing equipment. D_2O samples were prepared by lyophilizing an H_2O sample, and subsequently dissolving it in D_2O. The pH (uncorrected meter reading) was adjusted to 5.03 by the addition of microliter quantities of 0.1 M solutions of DCl and NaOD.

NMR Spectroscopy. ^1H NMR spectra were recorded on Bruker AMX 500 and AMXT 600 spectrometers. All 2D spectra were recorded in the pure-phase absorption mode by application of TPPI (Marion & Wüthrich, 1983). The proton spectral width was set to 14 ppm. Water suppression was achieved by irradiation of the water resonance during 1.0 s. The recording temperature was 25 °C. The proton ppm values were calibrated using the water resonance, with a chemical shift of 4.75 ppm relative to 3-(trimethylsilyl)propionate; nitrogen chemical shifts were referred to the NH_4Cl signal at 22 ppm. A DQF-COSY spectrum (Bax & Davis, 1985) was recorded at 500 MHz in D_2O and a regular COSY spectrum in H_2O, both with high resolution in ω_2. NOESY spectra in H_2O were recorded at 600 MHz with mixing times of 75 and 150 ms; 512 t_1 values of 2048 data points were acquired. A NOESY spectrum in D_2O was recorded at 500 MHz with a 75-ms mixing time. Clean TOCSY spectra (Griesinger et al., 1988) were recorded with mixing times of 32 and 64 ms for measurements in H_2O at 600 MHz. Data were processed on a Silicon Graphics IRIS workstation using the "TRITON" software. Typically, the data were processed with sine-bell or square sine-bell window functions shifted over $\pi/6$ in ω_2 and $\pi/3$ in ω_1. Linear prediction was used in the ω_1 direction (Olejniczak & Eaton, 1990). Additional zero-filling was used to obtain a spectral data matrix of 1K × 1K. Base-line corrections were carried out with a fourth-order polynomal function.

The heterocorrelation experiments were recorded on AMX 500 and AMXT 600 spectrometers using a 5-mm ^1H broad-band inverse probe, using fast switching on the proton channel for presaturation and hard pulses. The heteronuclear *J*-coupling refocusing delay was set to 4 ms. HMQC spectra (Müller, 1979) and HSQC spectra (Bodenhausen et al., 1980) were recorded with the ^{15}N carrier in the center of the amide region with a ^{15}N spectral width of 29 ppm. The Nϵ protons of the arginine side chain were folded in the spectrum. A 3D NOESY-HSQC was recorded with a 150-ms mixing time (Marion et al., 1989) (220 real, 96 real, 512 complex data points). The 3D dataset was processed as described for the 2D spectra with linear prediction both in ω_1 and in ω_2, resulting in a data set $(\omega_1, \omega_2, \omega_3) = (512, 128, 512)$ on a Silicon Graphics IRIS workstation. The 512 data points in ω_3 cover the amide proton region downfield with respect to the water resonance (the upfield half was discarded after Fourier transformation in ω_3). A 3D HMQC-NOE-HMQC experiment was recorded with a 75-ms mixing time (Ikura et al., 1990) (64 real, 64 real, 512 complex data points).

Slowly exchanging amide protons were identified in HMQC spectra at 500 MHz of the ^{15}N-labeled protein dissolved in D_2O. The sample was prepared by lyophilization of the H_2O sample of the ^{15}N-labeled protein. Subsequently, the protein was dissolved in D_2O. The first experiment was started after 5 min, and its recording took 15 min. Hereafter, a second HMQC spectrum was recorded in 50 min. A third HMQC spectrum was recorded after 18 h of incubation of the sample in D_2O at room temperature.

RESULTS AND DISCUSSION

The POU_s protein is efficiently expressed in the pET-15^b expression system in a soluble form. The purification is facilitated by the presence of the His-tag, which allows for the application of affinity chromatography. The removal of this moiety proved to be easy. On polyacrylamide gel electrophoresis, the protein migrated as a single band. Verrijzer et al. (1992) showed that the POU_s protein is functionally active as a sequence-specific DNA-binding protein, albeit with low affinity.

The POU_s protein consists of 80 amino acids. The first four N-terminal residues are derived from the construct and are not an integral part of the Oct-1 protein. Residues 1–71 are part of a highly conserved region among the POU proteins (Rosenfeld, 1991), and residues 72–76 are part of the linker sequence, which connects the POU_s with POU_{hd} in the POU protein.

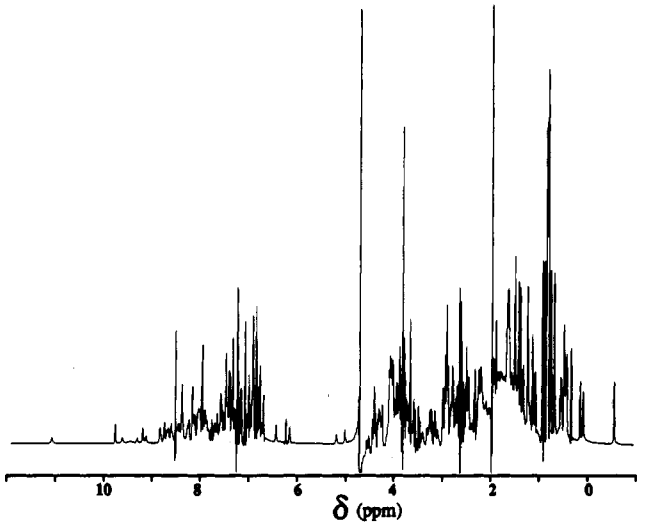

FIGURE 1: ^1H NMR spectrum of POU_s in H_2O at 600 MHz. Conditions: 3 mM protein, 0.1 M NaCl, 5 mM DTT, pH 5.03 at 298 K.

In initial experiments, the conditions of pH, salt concentration, and temperature were optimized for NMR. It became evident that POU_s is stable over a wide range of pH (7–3). Only under very acidic conditions (pH <3) did the protein unfold, as judged by the disappearance of high-field-shifted methyl resonances in the NMR spectrum. The unfolding process is reversible. The POU_s is temperature-sensitive, and although NMR resonance lines are fairly sharp at 319 K, the stability of the protein limits 2D experiments to 298 K. 2D experiments carried out at higher temperatures showed severe line broadening due to inhomogeneity in the sample, caused by denatured protein. No large changes in line width are observed with varying concentrations of protein (0.6–4 mM) or of salt (0.05–0.5 M NaCl). We find that POU_s at a concentration of 4 mM in 0.1 M NaCl/5 mM DTT at pH 5.03 and 298 K gives good NMR spectra. The 1D proton spectrum under these conditions is depicted in Figure 1. In the 1D spectrum, the amide chemical shift dispersion is low, which is an indication for α-helical secondary structure. The absence of CαH–CαH cross-peaks in the NOESY spectrum indicates that the protein contains no large stretches of β-sheet.

The essential step in the structural analysis with NMR is the assignment of all resonances in the spectrum. Therefore, we recorded proton COSY, TOCSY, and NOESY spectra in D_2O and H_2O solutions. Typical TOCSY and NOESY spectra are shown in Figure 2. In the TOCSY spectrum, 77 spin systems could be identified. In the region displayed in Figure 2, no signals can be expected for the N-terminal Gly(–4), nor for Pro61, so in this spectrum only one amide proton, of Ser39, is not identified. For many residues, the spin system could be partly or completely traced back on the amide line in the TOCSY spectrum in H_2O. The NOESY spectrum contains 76 of the 77 expected amide proton signals. No NOEs were observed for the resonance of Ser(–3), most likely due to high mobility in this region. In the amide proton region, numerous sequential N_i–N_{i+1} contacts are observed. Also, there are only few Hα protons which are relatively downfield-shifted. This is a strong indication of a high α-helix content of the protein.

Aromatic Residues. In Figure 3, the aromatic region of the COSY and NOESY spectra is shown. In the COSY spectrum, the correlations are indicated for the unique Trp66 and Tyr34. Furthermore, the spin systems of the six phenylalanines can be assigned, of which two show degeneracy in chemical shifts. In the NOESY spectrum, a number of interresidual NOEs can be observed linking two phenylalanines with residue Trp66. The sequential assignment of these three residues will be discussed in detail now.

The spin system of the unique Trp66 was identified in the COSY spectrum on the basis of three cross-peaks connecting the four ring protons H4, H5, H6, and H7. All four protons

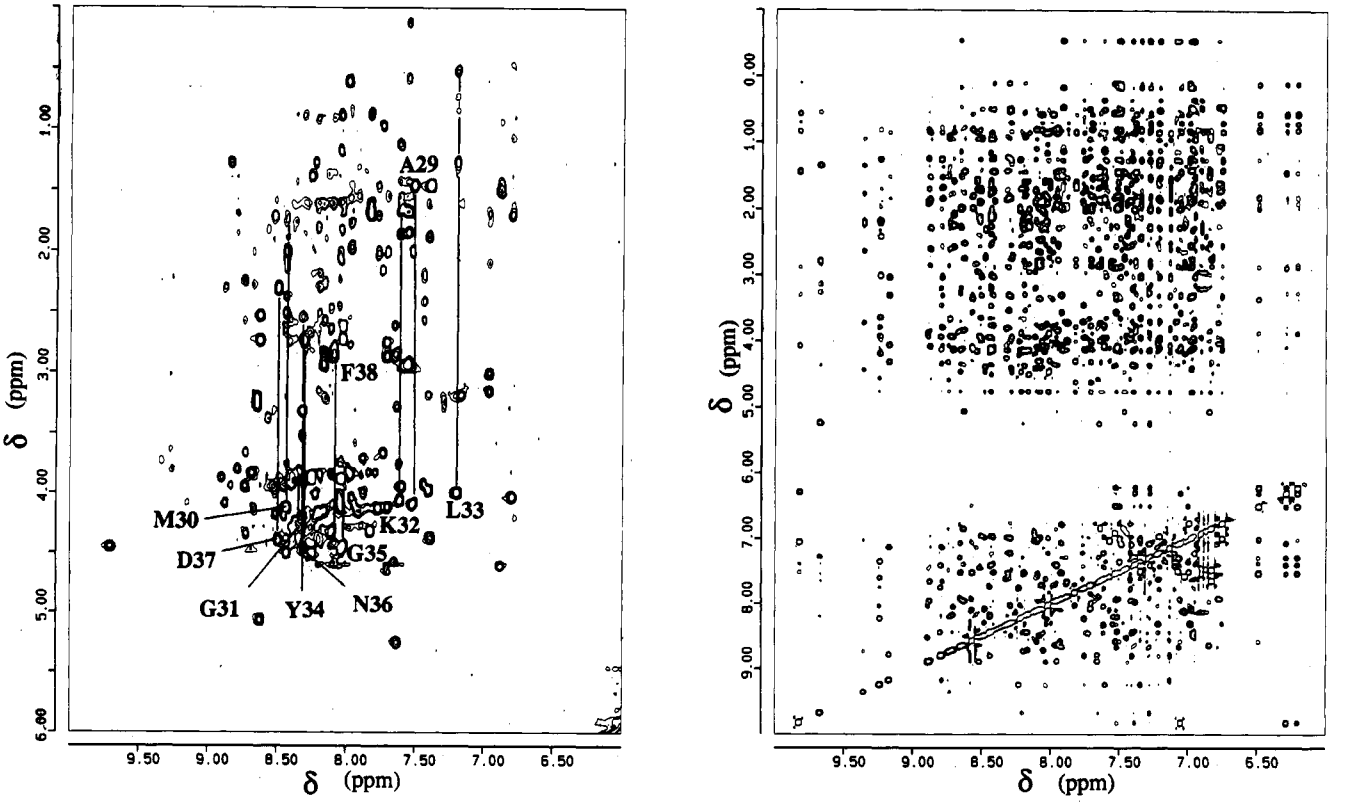

FIGURE 2: TOCSY spectrum (left panel) and 2D NOE spectrum (right panel) of POU_s at 600 MHz (for conditions, see Figure 1). The mixing times are 64 and 150 ms, respectively.

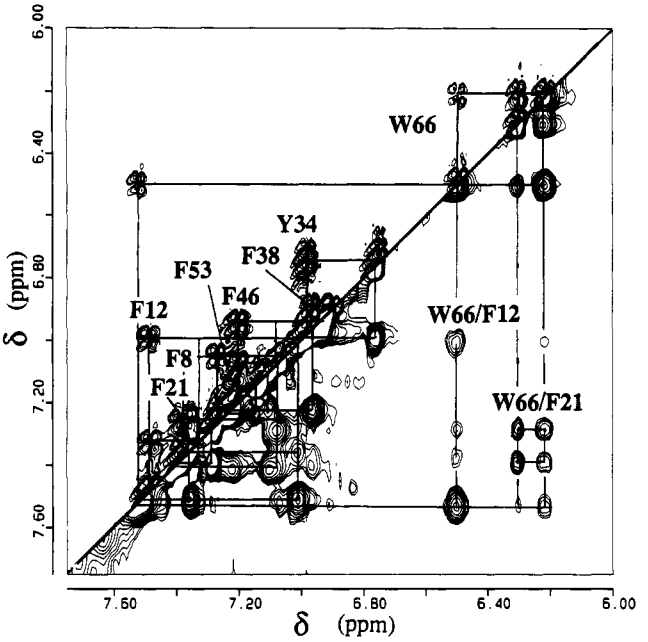

FIGURE 3: Aromatic region of the DQF-COSY spectrum (above the diagonal) and of the NOESY spectrum in D_2O with a 75-ms mixing time (below the diagonal) at 500 MHz (for conditions, see Figure 1). The spin systems of Trp, Tyr, and Phe are indicated in the COSY spectrum. In the 2D NOE spectrum, interresidual NOEs between Phe12, Phe21, and Trp66 are indicated.

have mutual NOE cross-peaks. The H2 was identified as a sharp resonance at 7.05 ppm with a strong NOE cross-peak with the indole proton resonating at 9.82 ppm. The NOE between H7 (6.29 ppm) and H2 is also present in the NOESY spectrum. Knowing the position of H7, the resulting assignments of the H4, H5, and H6 protons are 7.52, 6.49, and 6.21 ppm, respectively. The H2 and H4 ring protons displayed NOE cross-peaks with their amide, Hα, and the two Hβ protons (7.93, 4.07, 3.55, and 3.29 ppm).

For the second residue of the aromatic cluster, the phenylalanine with aromatic resonances at 7.41 and 7.29 ppm, the corresponding Hβ protons were identified on the basis of intraresidual NOE cross-peaks to the aromatic resonances. The NOEs with the H2,6 proton are strong, whereas the NOEs with the H3,4,5 protons are rather weak. Similar intensities were found for the aromatic protons to the Hα proton. In TOCSY and COSY spectra, the spin system was connected from Hβ and Hα to the amide proton at 7.65 ppm. The sequential α–N NOE with a threonine residue is very strong. The amide proton of this threonine was linked in COSY and TOCSY spectra to the side-chain protons (Hα,Hβ, and Hγ). The residue preceding the phenylalanine was linked by sequential N–N and Hα1,Hα2–N NOEs, and was identified as a glycine (NH, Hα1, and Hα2 at 7.88, 3.71, and 3.98 ppm). The Gly-Phe-Thr sequence occurs only once, sequentially pinpointing this phenylalanine to residue 21.

In a similar manner, the amide of the second phenylalanine (H2,6, H3,5, and H4 at 7.36, 7.51, and 7.01 ppm) was assigned at 9.24 ppm. Sequential NOEs positioned this residue in the sequence Thr-Phe-Lys, leading to the assignment of Phe12. Thus, the three aromatic residues which display mutual NOEs are Trp66, Phe12, and Phe21. The sequential assignment of the remaining phenylalanines (8, 38, 46, and 53) and of Tyr34 was accomplished in a similar manner as discussed above. Residues Phe21, Phe38, and Phe53 show degeneracy in chemical shifts for the aromatic protons.

Sequential Assignment. The sequential assignment of backbone protons (NH, Hα) was carried out partly by following the NOE-based procedure as outlined by Wüthrich (1986) and partly by use of heteronuclear experiments. The assignment of the side-chain proton resonances was accomplished on the basis of *J*-correlated experiments (COSY and TOCSY).

Since the gene coding for POU_s is cloned and expressed in *E. coli*, we have been able to uniformly label the protein with ^{15}N. The ^{15}N-labeled protein enabled us to overcome the problems of spectral crowding encountered in the 2D homonuclear experiments. A 3D NOESY-HSQC experiment was recorded and analyzed. In this spectrum, the amide resonances are present with NOEs from the amide protons to intra- and interresidual protons. The intraresidual connectivities were assigned on the basis of the corresponding cross-peaks in the 2D TOCSY spectrum. The remaining NOEs arise from short-range distances linking the amino acids sequentially, or are medium- or long-range NOEs. With this strategy, many amino acids could be sequentially assigned, whereas in the 2D homonulear spectra alone this could not be accomplished due to extensive overlap. As an example, the sequential assignment of Ala29–Phe38 will be discussed below.

The spin systems of residues 29–38 were identified in the 2D TOCSY spectrum (Figure 2, left panel). As indicated by vertical lines, cross-peaks were observed from the amide proton resonances to the aliphatic protons. For Ala29 and Met30, cross-peaks were observed from the amide NH to the Hα and Hβ resonances. Gly31 gave rise to two signals, from the amide NH to both Hα's. For Lys32 and Leu33, cross-peaks could be identified from the amide NH to the Hα, Hβ, Hγ, and Hδ protons. Cross-peaks were observed from the amide NH to both Hα's for Gly35, and for Tyr34, Asn36, Asp37, and Phe38, cross-peaks from NH to Hα and Hβ protons were found.

The spin systems were easily traced back in the 3D NOESY-HSQC spectrum. In Figure 4, the ω_2 planes with ^{15}N frequency of the amide nitrogen of residues 29–38 are shown. For simplicity, only a narrow strip of these planes, containing the amide proton resonance of the residue, is selected. This allows a clear presentation of the sequential assignment. On the amide line of Ala29, the signals at 4.06 and 1.44 ppm are intraresidue cross-peaks to Hα and Hβ protons. Sequential contacts from Leu28 are also observed as indicated by arrows. Sequential N–N contacts to Leu28 and Met30 can be observed. The N–N contact from Ala29 to Met30 can also be seen at the amide line of Met30. At this amide proton, apart from the intraresidue contacts, sequential α–N and β–N contacts with Ala29 can be observed, as well as an N_i–N_{i+2} contact with Leu28. Met30 has sequential N–N, α–N, β–N, and γ–N contacts with Gly31. Also, N_i–N_{i+2} contacts with Ala29 and Leu33 are observed for Gly31, as well as a contact with the H2,6 protons of Tyr34 at 6.99 ppm. The amide proton of Lys32 has cross-peaks to its Hα, Hβ, Hγ, and Hδ protons, and to its Hϵ proton at 2.94 ppm. Both Hα protons from Gly31 are observed, as well as sequential N–N contacts with Gly31 and Leu33. The Hα and Hβ of Lys32 also appear at the amide proton position of Leu33. The Hγ of Lys32 has only a weak contact with Leu33. All aliphatic protons of Leu33, as well as the NH, have sequential contacts with the NH of Tyr34. The amide proton of Tyr34 has NOEs with its Hβ, but not with the Hα. This cross-peak is bleached out since the Hα coincides with the H_2O line at 4.75 ppm. A strong intraresidue NOE with its H2,6 protons can be observed, as well as a weak NOE with its H3,5 protons. An $H_{\beta i}$–N_{i+2} and a N_i–N_{i+2} contact with Lys32 could be identified. Sequential contacts from Tyr34 Hβ, HN, and H2,6 with the amide proton of Gly35 can be identified. Furthermore, (i,i+2) contacts from Leu33 Hβ and HN protons, as well as (i,i+3) contacts from Lys32 Hα, Hβ, and HN protons, can be observed

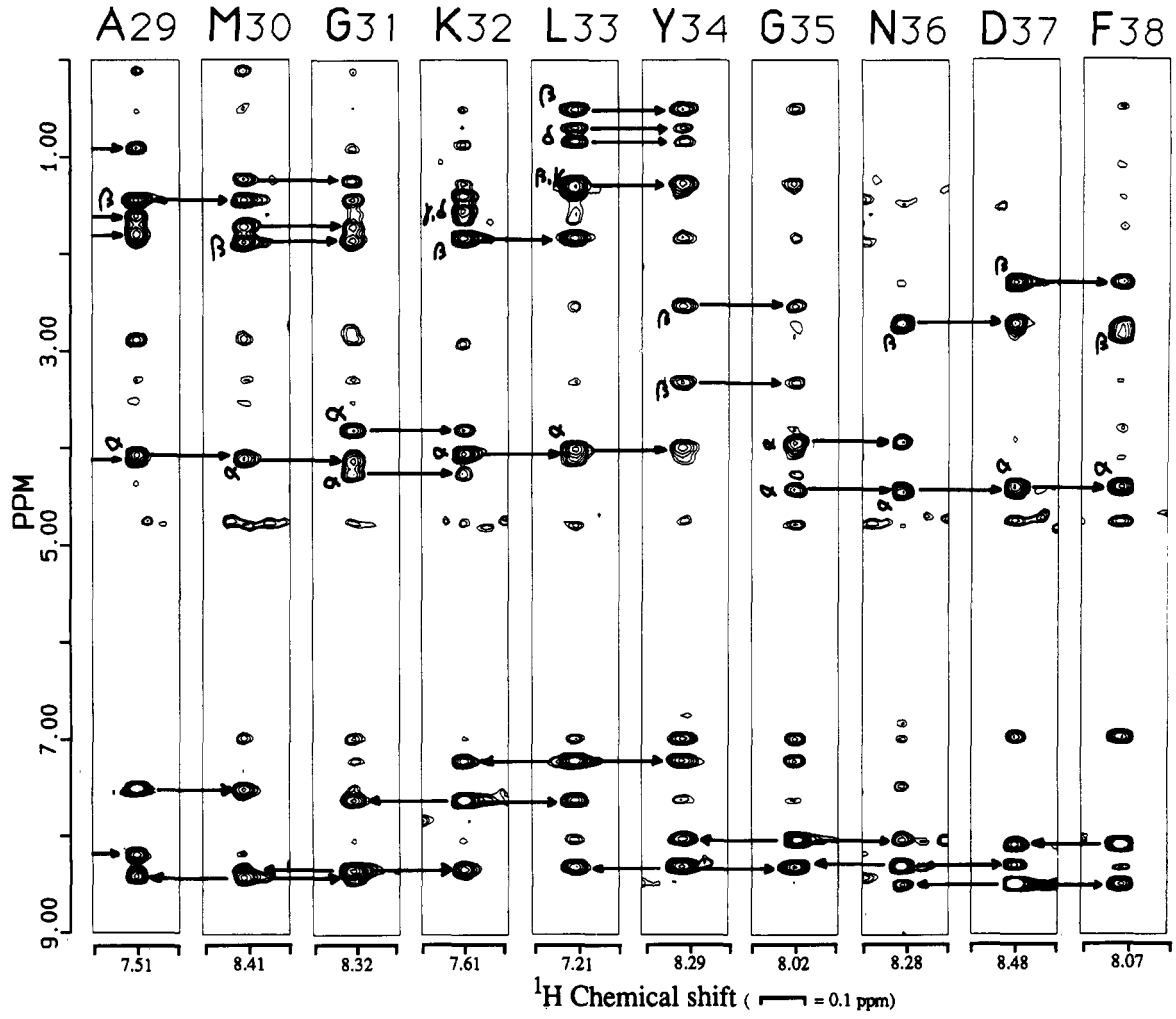

FIGURE 4: Sequential assignment of Ala29–Phe38 in the 600-MHz 3D NOESY-HSQC spectrum. Shown are slices from the 2D NOE planes. The intraresidual α_i–β_i NOE cross-peaks were identified by identical connectivities in the TOCSY and COSY spectra. The sequential NOE connectivities are indicated with arrows.

at the amide HN of Gly35. The amide proton of Asn36 has NOEs with its own Hα and Hβ and also weak NOEs with its side-chain amino group protons. Sequential contacts are observed from Gly35 Hα and HN protons. The sequential steps from Asn36 to Asp37 and from Asp37 to Phe38 include N–N, α–N, and β–N contacts. Finally, the H2,6 protons of Phe38 show contacts with its own amide proton as well as with the amide proton of Asp37.

In a similar manner, the sequential assignments were carried out for the residues (–3)–28 and 39–76. The unambiguous assignment of sequential amide–amide NOEs was carried out in a 3D HMQC-NOE-HMQC experiment. The spectrum allowed the assignment of NOEs between amide protons with identical or almost identical chemical shifts. This situation occurs 8 times in POU$_s$, for instance, the sequential step Met30–Gly31 (Figure 4). The amide–amide connectivity is clearly visible as a shoulder on the HMQC peak, but an estimation of the intensity is not possible. In the 3D HMQC-NOE-HMQC spectrum, all eight sequential steps were identified, and as an example, the connectivity for Asn68–Asp69 is shown in Figure 5. The amide protons both have a proton chemical shift of 8.09 ppm, but the resonances are resolved with respect to their nitrogen chemical shifts (113.4 and 116.6 ppm, respectively). The list of chemical shifts of the proton and nitrogen resonances is given in Table I.

Amide Proton Exchange. In the HSQC spectrum shown in Figure 6 (bottom), 75 well-separated cross-peaks are present, which all could be assigned on the basis of sequential connectivities in the 3D NOESY-HSQC spectrum. The

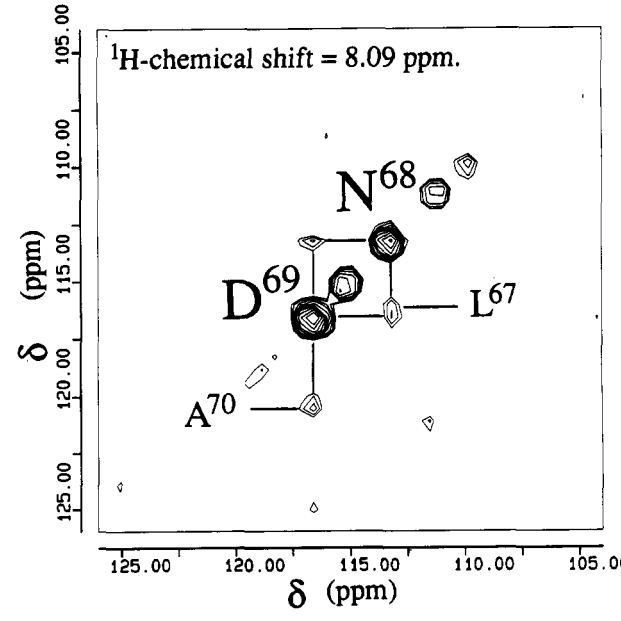

FIGURE 5: 3D HMQC-NOE-HMQC spectrum recorded on ^{15}N-labeled POU$_s$ at 500 MHz with a mixing time of 75 ms. Shown is the ω_1–ω_2 plane at a proton chemical shift of 8.09 ppm. In this plane, the sequential amide–amide NOE in between Asn68 and Asp69 is clearly present, which otherwise would not be observed.

HSQC cross-peaks of Leu19 and Asn72 overlap in the spectrum, and no resonances were found for the N-terminal residues Gly(–4) and Ser(–3). POU$_s$ contains one proline,

Table I: POU-Specific Domain: Chemical Shifts List[a]

residue	^{15}N amide	NH	Hα	Hβ	others	residue	^{15}N amide	NH	Hα	Hβ	others
–4 Gly						39 Ser	113	8.12	4.56	4.17	
–3 Ser		8.25	4.50	3.88		40 Gln	117.1	9.25	3.78	2.18, 2.23	Hγ, 2.32; NHε, 6.91, 7.44; ^{15}Nδ, 108.1
–2 His	117.3	8.66	4.75	3.19, 3.27	H4, 7.29; H2, 8.56						
–1 Met	118.9	8.43	4.50	1.99	Hγ, 2.50; Hε, 2.03	41 Thr	109.5	8.04	4.07		Hγ, 1.16
1 Asp	118.0	8.16	4.81	2.82, 2.95		42 Thr	115.7	7.62	3.75	4.07	Hγ, 1.09
2 Leu	118.4	8.54	4.15	1.70	Hγ, 1.57; Hδ, 0.81, 0.96	43 Ile	114.7	7.72	3.64	2.14	H_2γ, 1.23, 1.80; H_3γ, 0.95; H_3δ, 0.49
3 Glu	115.7	8.43	4.10	2.06, 2.13	Hγ, 2.36						
4 Glu	116.4	8.20	4.14	2.15, 2.29	Hγ, 2.52	44 Ser	111.5	8.45	4.16	3.93	
5 Leu	118.0	8.05	4.14		Hβ, Hγ, 1.58, 1.78; Hδ, 0.85	45 Arg	116.4	8.44	4.12	1.66, 1.73	Hγ, 2.09; Hδ, 3.00, 3.14; Hε, 6.94; ^{15}Nε, 81.1
6 Glu	115.7	8.71	3.93	2.08, 2.24	Hγ, 2.57						
7 Gln	114.7	8.17	4.13	2.25	Hγ, 2.54, 2.44; NHε, 6.90, 7.52; ^{15}Nδ, 108.8	46 Phe	118.0	8.51	3.97	3.02, 3.30	H2/6, 6.96; H3/5, 7.22; H4, 7.11
8 Phe	117.3	8.43	4.35	31.9, 3.45	H2/6, 7.41; H3/5, 7.29; H4, 7.08	47 Glu	112.7	8.41	3.75	2.11	Hγ, 2.44
9 Ala	118.6	8.80	3.93	1.26		48 Ala	114.7	7.39	4.36	1.44	
10 Lys	113.6	7.75	4.12	1.97, 2.01	Hγ, 1.45; Hδ, 1.69; Hε, 2.96	49 Leu	113.6	7.96	3.82	1.69, 1.93	Hγ, 1.44; Hδ, 0.78, 0.86
11 Thr	112.9	8.23	3.99	4.19	Hγ, 1.26	50 Asn	112.0	8.63	5.0–5	2.51, 2.74	NHδ, 6.83, 7.45; ^{15}Nγ, 106.7
12 Phe	120.7	9.24	3.64	2.41, 3.01	H2/6, 7.36; H3/5, 7.51; H4, 7.01	51 Leu	113.8	6.84	4.60	1.49	Hγ, 1.37; Hδ, 0.89, 0.95
13 Lys	115.0	7.60	3.93	1.95	Hγ, Hδ, 1.72	52 Ser	113.4	8.74	4.31	4.08	
14 Gln	111.1	7.44	3.93	2.12, 2.19	Hγ, 2.40, 2.55; NHε, 6.86, 7.44; ^{15}Nδ, 107.9	53 Phe	120.7	9.17	4.05	3.03, 3.31	H2/6, 7.13; H3/5, 7.24
						54 Lys	114.3	8.79	3.78	1.84	Hγ, 1.52; Hβ, Hν, 1.67; Hε, 2.99
15 Arg	116.1	8.51	3.92	1.71, 1.89	Hδ, 2.93, 3.20; Hε, 8.15; ^{15}Nε, 81.3	55 Asn	115.0	7.66	4.56	2.59, 2.84	NHδ, 7.07, 7.48; ^{15}Nγ, 109.2
16 Arg	117.5	8.89	3.87	1.89	Hγ, 1.25; Hδ, 2.73, 2.85; Hε, 11.15; ^{15}Nε, 80.6	56 Met	116.6	8.87	4.07	1.86	Hγ, 2.28; Hε, 1.53
						57 Cys	111.8	7.95	3.82	2.52, 2.76	
17 Ile	115.7	8.03	3.73	1.82	H_2γ, 1.03; H_3γ, 0.90; H_3δ, 0.85	58 Lys	115.2	7.42	3.95	1.86	Hγ, 1.24; Hδ, 1.48, 1.61; Hε, 2.83
18 Lys	119.3	7.96	4.02	1.94	Hγ, 1.52; Hδ, 1.71; Hε, 2.97						
19 Leu	113.8	7.70	4.11	1.53, 1.97	Hγ, 1.80; Hδ, 0.70, 0.79	59 Leu	112.5	7.62	3.93	1.12, 1.63	Hγ, 1.51; Hδ, 0.35, 0.50
20 Gly	102.8	7.88	3.71, 3.98			60 Lys	115.2	7.76	3.70		Hβ, Hγ, Hδ, 1.20, 2.00, 0.60, 0.70; Hε, 2.53
21 Phe	114.5	7.65	5.23	2.82, 3.26	H2/6, 7.29; H3/5, 7.41						
22 Thr	111.5	9.67	4.43	4.83	Hγ, 1.35	61 Pro			4.34	1.74, 2.24	Hγ, 1.91; Hδ, 3.45, 3.71
23 Gln	115.7	9.36	3.72	21.8, 2.24	Hγ, 2.63; NHε, 7.04, 8.10; ^{15}Nδ, 109.9	62 Leu	113.4	6.78	4.02	1.06, 1.69	Hγ, 1.61; Hδ, 0.46
						63 Leu	117.5	7.91	4.12	1.27, 1.52	Hγ, 1.13; Hδ, 0.17, –0.54
24 Gly	103.7	8.74	3.65, 3.93			64 Glu	116.1	8.66	4.12	1.98	Hγ, 2.26
25 Asp	119.6	8.20	4.36	2.77, 3.14		65 Lys	115.7	7.52	4.09	1.98	Hγ, 1.48, 1.53; Hδ, 1.68, 1.76; Hε, 3.03
26 Val	115.7	7.54	2.87	1.82	Hγ, 0.10, 0.55						
27 Gly	103.7	8.31	3.29, 3.52			66 Trp	115.9	7.93	4.07	3.29, 3.55	H2, 7.05; H4, 7.52; H5, 6.49; H6, 6.21;H7, 6.29; indole, 9.82; ^{15}N indole, 124.8
28 Leu	118.2	8.19	4.14	1.59, 1.79	Hγ, 1.68; Hδ, 0.91						
29 Ala	118.2	7.51	4.06	1.44							
30 Met	112.0	8.41	4.14		Hβ, Hγ, 1.25, 1.73, 1.88; Hε, 1.43	67 Leu	115.9	8.57	3.35	1.80, 1.98	Hγ, 1.80; Hδ, 0.81
						68 Asn	113.4	8.09	4.30	2.78, 2.84	NHδ, 7.03, 7.63; ^{15}Nγ, 108.8
31 Gly	106.0	8.32	3.85, 4.25			69 Asp	116.6	8.09	4.30	2.46, 2.63	
32 Lys	117.3	7.61	4.04	1.82	Hγ, 1.42, 1.52; Hδ, 1.60; Hε, 2.94	70 Ala	120.0	7.99	3.77	0.57	
						71 Glu	112.9	8.07	3.99	2.00	Hγ, 2.22, 2.44
33 Leu	113.8	7.21	3.99	0.50, 1.26	Hγ, 1.36; Hδ, 0.70, 0.84	72 Asn	113.8	7.71	4.61	2.75, 2.84	NHδ, 6.83, 7.63; ^{15}Nγ, 109.7
34 Tyr	111.3	8.29	4.80	2.54, 3.31	H2/6, 6.99; H3/5, 6.76	73 Leu	117.3	7.82	4.29	1.66	Hγ, 1.59; Hδ, 0.83, 0.88
35 Gly	105.8	8.02	3.92, 4.44			74 Ser	112.2	8.01	4.45	3.87	
36 Asn	112.0	8.28	4.46	2.69, 2.74	NHδ, 7.07, 7.47; ^{15}Nγ, 108.8	75 Ser	114.5	8.22	4.45	3.90	
37 Asp	114.7	8.48	4.38	2.30		76 Asp	123.5	8.02	4.44	2.60, 2.71	
38 Phe	115.2	8.07	4.38	2.76, 2.85	H2/6, 6.97; H3/5, 6.93						

[a] Chemical shifts (in ppm) of the assigned ^{1}H and ^{15}N resonances of the POU_s domain. ^{1}H chemical shifts are referred to the water signal at 4.70 ppm; ^{15}N chemical shifts are referred to the NH_4Cl signal at 22 ppm. Conditions: T = 298 K; pH = 5.0; [NaCl] = 0.1 mM; [DTT] = 5 mM.

which means that the HSQC spectrum contains all backbone resonances of residues His(–2)–Asp76. Side-chain resonances were identified for the indole NH of Trp66, and the three arginine Nε protons. The latter resonances were easily identified on the basis of their highfield ^{15}N chemical shifts of 80.6, 81.1, and 81.3 ppm. In the HSQC spectrum shown in Figure 6, these cross-peaks can be found at a ^{15}N chemical shift of around 117 ppm, due to folding. The POU_s protein has five asparagines and four glutamines. The side-chain amide protons are indicated in Figure 6 (bottom). All nine sets of two protons connected with one nitrogen could be identified with ^{15}N chemical shifts ranging from 104 to 109 ppm. The sequence-specific assignments were carried out on the basis of the strong intraresidual NOE connectivities for these NH_2 groups in the 3D NOESY-HSQC.

The HMQC experiment proved to be an excellent tool to study amide proton exchange. Figure 6 (top) shows the HMQC spectrum which was recorded on a freshly prepared sample in D_2O from a lyophilized H_2O sample. The spectrum contains 50 backbone amide resonances, and 2 side-chain resonances. In the spectrum, recorded 18 h after preparation of the sample, 19 backbone resonances remain present, identifying these amide protons as slowly exchanging. The intermediate and slow exchange of the amide protons is indicated in Figure 7 with open and filled circles, respectively. In addition to the backbone resonances, two side-chain resonances displayed intermediate exchange behavior. The side-chain indole proton of Trp66 and the Arg16 Nε proton were observed in the HMQC spectrum in D_2O. The assignment of these resonances was straightforward since the protons both have unique chemical shifts of 9.82 and 11.15 ppm (see also Figure 1). Many NOEs have been identified for the tryptophan indole ring (among these the NOEs with Phe12 and Phe21 indicated in Figure 3). This indicates that this aromatic residue has a buried position in the core of the molecule. The slow exchange of the indole proton can therefore be explained by either assuming shielding of the solvent or the presence of a hydrogen bond with this side chain. The Arg16 Nε proton has NOEs with the aromatic protons of Phe12, which may indicate an internally buried position for the side chain of this arginine, and the possible formation of an internal salt-bridge.

The most likely explanation for intermediate and slow exchange behavior is the involvement of the amide proton in a hydrogen bond. In a two-stranded β-sheet, the amide protons are alternatively involved in a hydrogen bond in between the

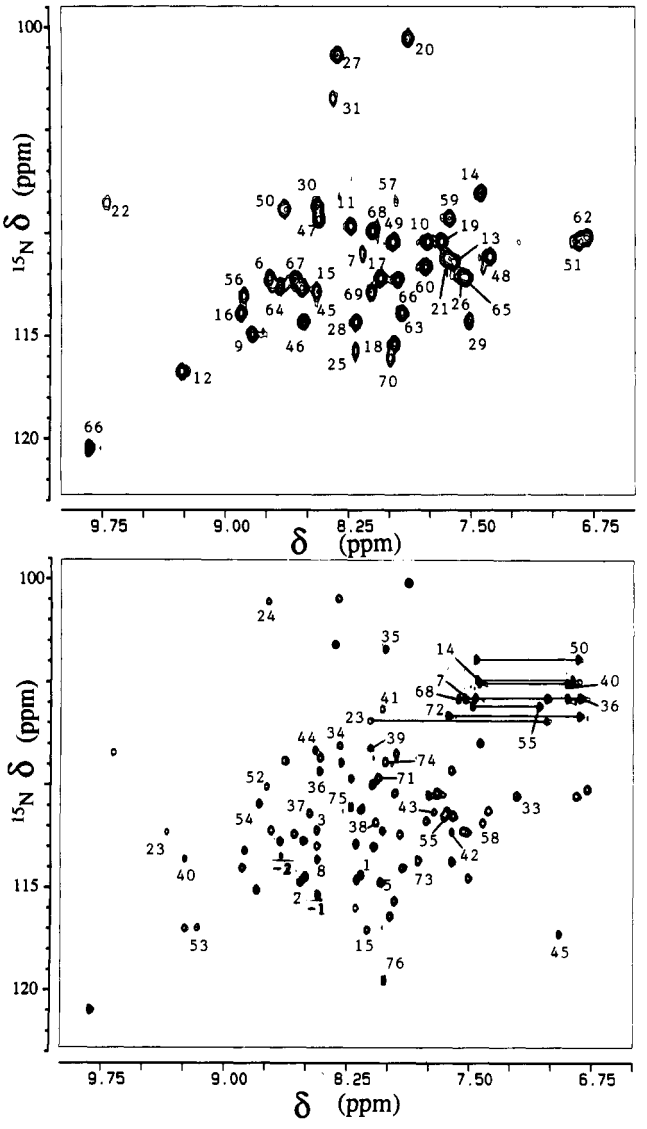

FIGURE 6: HMQC spectrum at 500 MHz (top) of ^{15}N-labeled POU$_s$ in D_2O and an HSQC spectrum at 600 MHz (bottom) of ^{15}N-labeled POU$_s$ in H_2O. (Conditions: 3 mM protein, 0.1 M NaCl, 5 mM DTT, pH 5.03 at 298 K.)

two strands, whereas the following amide proton is exposed to the solvent. This results in an alternating pattern of fast and slow amide proton exchange in the sequence. In an α-helix, the secondary fold is stabilized by the formation of hydrogen bonds between the carbonyl oxygen of residue i and the amide proton of residue i+4. This results in a continuous stretch of slowly exchanging amide protons starting with the fifth residue of the α-helix. In the sequence of POU$_s$ outlined in Figure 7, it is evident that there are four continuous stretches of residues which have amide protons involved in hydrogen bonds. These regions are Leu5–Thr22, Asp25–Tyr34 (lacking residue Lys32), Ser44–Leu51, and Met56–Glu71. These results indicate the presence of four helices. Within these helices, the amide protons, which display slow exchange, are all located in the central regions, with the exception of Val26, whereas the residues displaying intermediate exchange are present at both ends of the helices.

Secondary Structure. On the basis of the resonance assignments, a large number of sequential and medium-range NOE cross-peaks could be identified in the 2D NOESY, 3D NOESY-HSQC, and 3D HMQC-NOE-HMQC spectra. Cross-peaks in the 2D NOESY spectrum, which had been recorded with a 75-ms mixing time, were classified into three different catagories: strong, medium, and weak intensities.

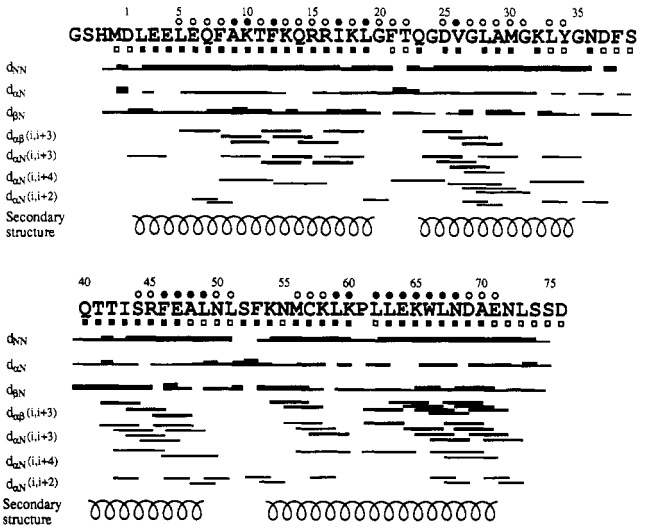

FIGURE 7: Sequential and medium-range NOE contacts observed in the 2D NOE and 3D NOESY-HSQC spectra of POU$_s$. The thickness of the horizontal bars is a qualitative indication of the relative intensity of the NOE as observed in the 2D NOE spectra, as discussed in the text. In the case of proline residues, NOEs pertain to the Hδ protons rather than to the backbone NH proton. The slow exchange of amide resonances is indicated with filled circles, whereas open circles represent intermediate exchange. Filled and open boxes denote small (<7 Hz) and large (>8 Hz) $^3J_{HN\alpha}$ coupling constants, respectively.

Additional cross-peaks present in the 2D NOESY and 3D NOESY-HSQC spectra with a mixing time of 150 ms were classified as being very weak. The intensities of the sequential and medium-range connectivities are summarized in Figure 7. Analysis of NOE connectivities, $^3J_{HN\alpha}$ coupling constants, and amide proton exchange behavior provides information on secondary structure elements. The characteristic NOE connectivity pattern for an α-helix is the presence of strong sequential N_i–N_{i+1} and medium α_i–N_{i+1} NOEs in combination with medium α_i–β_{i+3} and weak α_i–N_{i+3} medium-range contacts. The NOE pattern should coincide with slowly exchanging amide protons and with small $^3J_{HN\alpha}$ coupling constants (4 Hz) in such a region. The secondary structure elements derived for POU$_s$ from the analysis of the NOE and amide exchange data will now be discussed in detail.

(*A*) *Gly(–4)–Met(–1).* The first four residues adopt no regular secondary structure. For Gly(–4) and Ser(–3), no NOEs could be identified, which indicates high local mobility for these residues. To a lesser extent, this is also found for residues His(–2) and Met(–1), since the NOE intensities here are rather low. The sequential step from Met(–1) to Asp1 is characterized by a strong $d_{\alpha N}$, which indicates an extended backbone conformation.

(*B*) *Helix I: Asp1–Leu19.* The first helix in POU$_s$ extends from Asp1 to Leu19. Sequential and medium-range NOEs in combination with slow exchange for residues 5–19 all agree with this. The α_i–β_{i+3} and α_i–N_{i+3} contacts are found up to residue Leu19; hereafter, these medium-range contacts are not observed. Small $^3J_{HN\alpha}$ coupling constants are observed for residues 2–19.

(*C*) *Loop I: Gly20–Thr22.* No i,i+3 connectivities are observed for residues 20–22, and residues 21 and 22 display a strong α–N contact, whereas the N–N contact is clearly absent. Therefore, this segment is present in an extended structure, as is further evidenced by large $^3J_{HN\alpha}$ coupling constants for residues 21 and 22. For the regular turn, we would expect a hydrogen bond between the carbonyl of residue i and the amide proton of residue i+3, but neither Gln23 nor Gly24 shows slow exchange of its amide proton. These

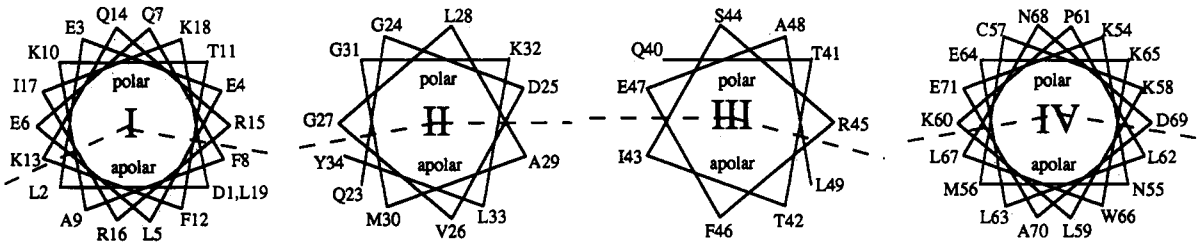

FIGURE 8: Helical wheel presentation of the four helices present in POU_s.

observations indicate that residues Gly20–Thr22 are present in an irregular loop whereas hydrogen bond formation can possibly be accomplished by backbone/side-chain interactions, or interactions with the carboxy-terminal residues of the preceding helix.

(*D*) *Helix II*: *Gln23–Tyr34*. The second helical region starts at Gln23. From the α proton of this residue, NOEs to the β and amide protons of residue i+3 could be identified, and strong sequential N–N contacts were observed up to residue Tyr34. These connectivities were identified in the 3D HMQC-NOE-HMQC spectrum for the sequential steps Gly27–Leu28 and Met30–Gly31, since the amide resonances of the residues involved have almost identical chemical shifts. The residues Asp25 and Val26 both show slow amide exchange behavior, which may indicate an extension of the helix at the N-terminus. However, there is only one additional NOE connectivity [Phe21(α)–Asp25(N)], and this involves the loop residue Phe21. At this stage, we are not certain of the hydrogen bond acceptors which are involved with the hydrogen bonds of residues 25 and 26. Small $^3J_{HN\alpha}$ coupling constants were observed for residues 23–32, except for the glycines.

(*E*) *Loop II*: *Gly35–Ser39*. At residue Gly35, helix II stops, which we can conclude from the absence of slow exchange for the five residues 35–39 and from the large $^3J_{HN\alpha}$ coupling constants for residues 37–39. For this loop region, no regular NOE pattern has been identified.

(*F*) *Helix III*: *Gln40–Leu49*. The third helix is characterized by slow exchange for the amide protons of residues 44–49. Furthermore, medium-range NOEs of the (i,i+3) and (i,i+4) type have been assigned starting with residue 41 up to residue 49. Strong sequential N–N NOEs were assigned for residues 40–49. The sequential N–N connectivities for the amides of Arg45, Phe46, and Gln47 could be assigned in the 3D HMQC-NOE-HMQC. Small $^3J_{HN\alpha}$ coupling constants are observed for residues 40–47.

(*G*) *Loop III*: *Asn50–Phe53*. An extended structure with medium and strong sequential α–N contacts is found for residues Asn50–Phe53. We found no experimental basis for the presence of a regular turn in this region.

(*H*) *Helix IV*: *Lys54–Glu71*. A fourth helix is found at the C-terminus of POU_s. The amide protons at both ends (Met56–Lys58 and Asp69–Glu71) display intermediate exchange behavior, whereas residues located in the center of the helix (Leu59–Asn68) exhibit slow exchange. The helix is furthermore evidenced by the presence of 18 (i,i+3) contacts and 4 (i,i+4) contacts. The expected small $^3J_{HN\alpha}$ coupling constant is found for residues 56–70, only interrupted at Leu62. This can be accounted for by the presence of a proline at position 61, which introduces a kink in the helix, as will be discussed below.

(*I*) *Asn72–Asp76*. The last five residues in the sequence could be assigned, but no regular secondary structure is present. Residues Ser75 and Asp76 display narrow line widths, which indicates high mobility.

Figure 8 is the helical wheel presentation of the four α-helices. It is clear that all four helices are amphipathic. All charged residues are located on the polar surface, with two exceptions. Asp1 is an acidic residue, but its N-terminal position will not likely result in a burial of the charged side chain in the hydrophobic core of the protein. For residue Arg16, the situation is different; as already pointed out, the Nϵ proton is in intermediate exchange with the solvent, and this proton has NOEs to the aromatic ring protons of Phe12. The latter residue is located in the same helix, one turn before. This results in a buried charged guanidino group, the precise structural role will only become known after a complete analysis of the three-dimensional structure.

The apolar hydrophobic sides of the helices contain the amino acids whose side chains make up the hydrophobic core of the protein. As already discussed in the sequential assignments of the aromatic residues, NOEs have been identified among Phe12 (helix I) and Trp66 (helix IV), indicated in Figure 3. The determination of the complete three-dimensional structure of the protein is in progress.

It is noteworthy that helix II contains three glycine residues. Generally, due to the absence of a side chain, glycine allows more flexibility in the main chain. In helix II, this may be reflected in the absence of slowly exchanging amide protons (Val26 is not part of the regular hydrogen bond pattern). Moreover, the amide proton of residue Lys32 was not identified as being in intermediate exchange with the solvent. In the other three helices, the central part contains several amide protons, which are efficiently protected from exchange with the solvent. Helices III and IV contain core regions of four and nine sequential residues, which do display slow exchange behavior. In the first helix, residues 9, 10, 12, 17, and 19 display slow exchange. The hydrogen bonds made by the amide protons of residues 9, 12, and 19 are located at the apolar side of the helix, which demonstrates the differences in the strength of the hydrogen bonds at the polar and apolar sites of the helix.

In helix IV, a proline (Pro61) residue is present in the middle of the helix, and therefore no hydrogen bond is formed with the carbonyl of residue Met56. In spite of the absence of this hydrogen bond, the α-helix is strikingly stable in this region; the amide protons of residues 59–68 all are in slow exchange. The presence of a proline in a helix has already been observed, for instance in crystal structures of myoglobin (Kendrew et al., 1960) and adenylate kinase (Schulz et al., 1974). In these cases, the presence of a proline results in a kink in the helix with an angle of about 20°. Due to this kinking, the distances between residues i and i+3 increase. This may explain the absence of NOE contacts for the Hδ of Pro61 with residues 57 and 58. The structure of helix IV in POU_s will be determined both by the presence of the proline and by hydrophobic packing interactions of residues at the apolar site of the helix in the core of the protein, and this awaits the determination of the three-dimensional structure.

The sequence of POU_s is divided into two highly conserved boxes, the A-region and the B-region (Rosenfeld, 1991). The A-region contains residues 3–33, and includes helices I and II. The B-region contains residues 39–71, and covers helices

III and IV. Structural prediction methods indicated the presence of only two helical regions for residues 22–33 and 63–71 (Ingraham et al., 1990). These predictions have guided mutagenesis experiments to elucidate the role of POU_s in biological processes. It is now clear that the predictions for POU_s do not fit the results of our study. In particular, helix II was not predicted, presumably because of the presence of three glycine residues. Furthermore, only part of helix IV was correctly predicted. The determination of the three-dimensional structure is in progress.

REFERENCES

Bax, A., & Davis, D. G. (1985) *J. Magn. Reson. 61*, 306–320.

Botfield, M. C., Jancso, A., & Weiss, M. A. (1992) *Biochemistry 31*, 5841–5848.

Griesinger, C., Otting, G., Wüthrich, K., & Ernst, R. R. (1988) *J. Am. Chem. Soc. 110*, 7870–7872.

Ikura, M., Bax, A., Clore, M., & Gronenbron, A. (1990) *J. Am. Chem. Soc. 112*, 9020–9022.

Ingraham, H. A., Flynn, S. E., Voss, J. W., Albert, V. R., Kapiloff, M. S., Wilson, L., & Rosenfeld, M. G. (1990) *Cell 61*, 1021–1033.

Janknecht, R., de Martynoff, G., Lou, J., Hipskind, R. A., Nordheim, A., & Stunnenberg, H. G. (1991) *Proc. Natl. Acad. Sci. U.S.A. 88*, 8972–8976.

Kendrew, J. C., Dickerson, R. E., Strandberg, B. E., Hart, R. G., Davies, D. R., Phillips, D. C., & Shore, V. C. (1960) *Nature 185*, 422–427.

Kissinger, C. R., Liu, B., Martin-Blanco, E., Kornberg, T. B., & Pabo, C. O. (1990) *Cell 63*, 579–590.

Kristie, T. M., & Sharp, P. A. (1990) *Genes Dev. 4*, 2383–2396.

Marion, D., & Wüthrich, K. (1983) *Biochem. Biophys. Res. Commun. 113*, 967–974.

Marion, D., Kay, L. E., Sparks, S. W., Torchia, D. A., & Bax, A. (1989) *J. Am. Chem. Soc. 111*, 1515–1517.

Müller, L. (1979) *J. Am. Chem. Soc. 101*, 4481.

Olejniczak, E. T., & Eaton, H. L. (1990) *J. Magn. Reson. 87*, 628–632.

Qian, Y. Q., Billeter, M., Otting, G., Müller, M., Gehring, W. J., & Wüthrich, K. (1989) *Cell 59*, 573–580.

Rosenfeld, M. G. (1991) *Genes Dev. 5*, 897–907.

Ruvkun, G., & Finney, M. (1991) *Cell 64*, 475–478.

Schöler, H. R. (1991) *Trends Genet. 7*, 323–329.

Schulz, G. E., Elzinga, M., Marx, F., & Schinner, R. H. (1974) *Nature 250*, 120–123.

Studier, F. W., Rosenberg, A. H., Dunn, J. J., & Dubendorf, J. W. (1990) *Methods Enzymol. 185*, 60–89.

Sturm, R. A., Das, G., & Herr, W. (1988) *Genes Dev. 2*, 1582–1599.

Verrijzer, C. P., & van der Vliet, P. C. (1993) *Biochim. Biophys. Acta* (in press).

Verrijzer, C. P., Kal, A. J., & van der Vliet, P. C. (1990a) *EMBO J. 9*, 1883–1888.

Verrijzer, C. P., Kal, A. J., & van der Vliet, P. C. (1990b) *Genes Dev. 4*, 1964–1974.

Verrijzer, C. P., Alkema, M. J., van Weperen, W. W., van Leeuwen, H. C., Strating, M. J. J., & van der Vliet, P. C. (1992) *EMBO J. 11*, 4993–5003.

Wolberger, C., Verstow, A. K., Liu, B., Johnson, A. D., & Pabo, C. O. (1991) *Cell 67*, 517–528.

Wüthrich, K. (1986) *NMR of proteins and nucleic acids*, John Wiley & Sons, New York.